Investigation of Energy-Scaling of Thrust Performance for Laser Fusion Rocket

Taiki INATOMI, Naoji YAMAMOTO, Hideki NAKASHIMA, Yoshitaka MORI[1)], Toshiyuki ISE[2)], Shunsuke MURATA[2)], Kazuhiro YAGI[2)] and Taichi MORITA

Kyushu University, 6-1 Kasugakoen, Kasuga, Fukuoka 816-8580, Japan
[1)]*Graduate School for the Creation of New Photonics Industries, Hamamatsu, Shizuoka 431-1202, Japan*
[2)]*IHI Aerospace Co., ltd., 900 Fujiki, Tomioka, Gunma 370-2398, Japan*

(Received 22 March 2023 / Accepted 25 July 2023)

A laser fusion rocket has been proposed for interplanetary flight. This rocket generates a high-energy plasma via laser-fusion and expels it via a magnetic nozzle. The magnetic nozzle is a key component for the rocket performance, and we have investigated the impulse bit generated from the magnetic nozzle by using simulations and experiments in relatively low energy regime of a few joules. In addition, the energy dependence on the thrust performance is an essential factor to evaluate and design the laser fusion rocket. Here, we conducted numerical simulations in energy regimes from a few joules to mega joules to understand the thrust performance both for small-scale experiments and for full-scale fusion rockets. We find that the momentum efficiency does not depend on the propellant mass, material, and plasma energies, and the impulse bit is expressed as the power-law of the plasma energy and mass. These relations are important for designing missions and for estimating the thrust of fusion rockets.

Keywords: laser fusion rocket, magnetic nozzle, hybrid simulation, propulsion, thruster, energy scaling

DOI: 10.1585/pfr.18.1404080

1. Introduction

NASA is currently executing Artemis program which includes crewed lunar flights and construction of lunar orbiters. Next, a crewed mission to Mars is expected. Although various systems have been proposed for travelling to Mars, in general, it takes 9 - 12 months with the current propulsion systems [1]. This mission time needs to be shortened to decrease the harmful effects of a zero-gravity environment and from cosmic radiation. A laser fusion rocket (LFR) [2] has been proposed by R. A. Hyde [3, 4] to reduce this long mission time. In this rocket, a propellant is ionized and energized by inertial-confinement-fusion (ICF), and the high-energy plasma is controlled by a magnetic nozzle formed by a super-conducting coil. As a result, the rocket obtains a thrust as a reaction force. Various researches have been conducted to understand the performance of the magnetic nozzle. Nagamine *et al*. have investigated the thrust performance from a high-energy (4 MJ) gold (Au) plasma with numerical simulation [5]. Maeno *et al*. compared the simulation and experiment with the laser energy of 10 - 1000 J [6]. Morita *et al*. conducted experiments in various laser energies all less than 1000 J and investigated the similarity of the plasma structure [7]. The experiments have been performed with the energy of less than 10 J in most experiments, and it remains unclear how thrust performance varies on the plasma energy as the energy is scaled from a few joules (for experiments) to 62 MJ (for LFR) [8].

In this paper, we investigate the thrust performance of the magnetic nozzle in a wide range of plasma energy with three-dimensional hybrid simulations. We find that the thrust efficiency η does not depend on the plasma energy (E_p), species, or propellant mass (m_p). We also find that the impulse bit (I_b) is expressed as a power-law of energy and mass ($m_\mathrm{p}E_\mathrm{p}$) with the index of ~0.5, or in other words, the normalized impulse bit $I_\mathrm{b}/\sqrt{m_\mathrm{p}}$ is in the power-law of E_p.

2. Calculation Method

2.1 Hybrid simulation

We used a three-dimensional hybrid code [5] from prior work to calculate the plasma expansion in the magnetic nozzle. Ions were treated as super-particles and electrons were treated as an inertialess fluid. By assuming quasi-neutrality and using Darwin approximation, we ignored high-frequency and fast phenomena such as electron plasma waves and electromagnetic waves.

The following equations are solved in a Cartesian coordinate. The motion of ions and electrons are described below.

$$m_\mathrm{i}\frac{d\boldsymbol{v}_\mathrm{i}}{dt} = Ze(\boldsymbol{E} + \boldsymbol{v}_\mathbf{i} \times \boldsymbol{B}), \tag{1}$$

$$\frac{d\boldsymbol{x}_\mathbf{i}}{dt} = \boldsymbol{v}_\mathbf{i}, \tag{2}$$

author's e-mail: morita@aees.kyushu-u.ac.jp

$$n_e m_e \frac{d\boldsymbol{v_e}}{dt} = -en_e(\boldsymbol{E} + \boldsymbol{v_e} \times \boldsymbol{B}) - \nabla P_e, \tag{3}$$

where m_i and m_e are the ion and electron masses, respectively, and $m_e = 0$ is assumed here. $\boldsymbol{v_i}$ and $\boldsymbol{v_e}$ are the velocities of ions and electrons, respectively, $\boldsymbol{E}$ and $\boldsymbol{B}$ are the electric and magnetic fields, respectively, $\boldsymbol{x_i}$ is the position of an ion, and n_e is the electron density. P_e is the electron pressure expressed as

$$P_e = n_e T_e, \tag{4}$$

and Eq. (3) becomes

$$0 = -en_e(\boldsymbol{E} + \boldsymbol{v_e} \times \boldsymbol{B}) - \nabla (n_e T_e). \tag{5}$$

Ampere's law is expressed as

$$\nabla \times \boldsymbol{B_p} = \mu_0(\boldsymbol{j_i} + \boldsymbol{j_e}), \tag{6}$$

where $\boldsymbol{j_i}$ and $\boldsymbol{j_e}$ are the ion and electron currents, respectively, B_p is the magnetic field induced in the plasma, and the electron current is expressed as

$$\boldsymbol{j_e} = -en_e\boldsymbol{v_e}. \tag{7}$$

From Eqs. (5), (6), and (7), the electric field becomes

$$\boldsymbol{E} = \frac{1}{Zen_i}\left[\frac{1}{\mu_0}(\nabla \times \boldsymbol{B_p}) \times \boldsymbol{B} - \boldsymbol{j_i} \times \boldsymbol{B} - ZT_e \nabla n_i\right], \tag{8}$$

and the time-evolution of the magnetic field is expressed from Faraday's law:

$$\frac{\partial \boldsymbol{B}}{\partial t} = -\nabla \times \boldsymbol{E}. \tag{9}$$

In the simulation code, Eq. 9 is calculated via the leap-frog method [9]. The ion density and ion current are calculated using a particle-in-cell (PIC) method in each grid position. In order to prevent $\boldsymbol{E}$ from diverging, a lower threshold is set to n_i where the number of super-particles in a single mesh must be larger than 10. For vacuum region where n_i is less than the threshold, the Laplace equation is solved by successive over-relaxation (SOR) [10]. The Neumann boundary condition in which the first derivative of the field value is assumed to be zero, is applied to the plasma surface. Here, we assume that a high-temperature fusion plasma expands adiabatically and that the plasma becomes cold after the expansion. Therefore, the plasma energy is distributed only in kinetic energy, i.e. we assume $T_e = T_i = 0$.

2.2 Simulation conditions

As in Ref. [8], we assume the laser energy of 1 MJ, fusion gain of 200, and the energy conversion efficiency from the total output energy to the propellant as 31% (20% from alpha particles and 11% from neutrons), resulting in the propellant energy of 62 MJ. The plasma mass of 2.4 g is estimated from the specific impulse of 15000 s which is required to reach Mars in 90 days [8, 11].

The super-particles are initially distributed uniformly spherically in both space and velocity-space, having only radial velocity without random motion assuming $T_i = 0$. In this case, the number of particles at the radius r_i is $N_i(r_i)dr_i \propto r_i^2 dr_i$ and that at the velocity v_i is $N_i(v_i)dv_i \propto v_i^2 dv_i$. Using these relations, the velocity distribution is calculated as $N_i(v_i)dv_i = (3N/v_{max})\, v_i^2 dv_i$, where N is the total number of super-particles and v_{max} is the maximum velocity at the outer edge expressed as $v_{max} = (10E_p/3m_p)^{1/2}$, where the plasma energy is the sum of all super-particles:

$$E_p = \sum \frac{m_i v_i^2}{2}. \tag{10}$$

The minimum velocity is $v_{min} = 0$ at the center, and the averaged velocity is estimated as $v_{avr} = (2E_p/m_p)^{1/2}$. The total number of particles is $N = 10^7$ and is enough to accurately represent the velocity distribution discussed above. Here, the time-step and the grid size were set to satisfy Courant-Friedrichs-Lewy (CFL) condition: $\Delta t < \Delta x/V$ where V is the typical plasma velocity, and $\Delta t < 0.2/\omega_{ci}$ for numerical stability where ω_{ci} is ion cyclotron frequency.

Figure 1 shows the simulation model in this study. The Au or H plasma is set at $z = z_c$ in front of the electromagnetic coil with the radius of r_c and the center of the coil is at the origin ($z = 0$). The ratio of $r_c/z_c = 1$ is set for all conditions (I-III), and $z_c = r_c = 5$ m for the highest energy of 62 MJ. The external magnetic field is applied via a constant current in a circular solenoidal coil. The magnetic field energy is 5 times larger than the plasma energy as consistent with Ref. [5] to obtain the maximum momentum efficiency.

We conducted the following three simulation conditions:

I Au plasma with 8 different energies with the average velocity of 227 km/s and the mass density of 3.0×10^{-4} kg m^{-3}.

II Au plasma with 8 different energies with the average velocity of 71.8 km/s and the mass density of 3.0×10^{-3} kg m^{-3}. Here, the propellant mass is 10 times larger than that used in the condition I.

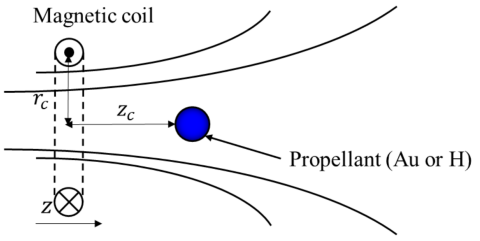

Fig. 1 Schematic diagram of the simulation. The magnetic field is applied externally with a single-turn coil, and the plasma is located on the central axis of the coil at the distance z_c.

Table 1 The simulation parameters for 8 different energies and three conditions: I-III.

				Au (I)		Au (II)		H (III)	
E_p [J]	r_c [m]	I_c [kA·turn]	B_c [T]	m_p [g]	v_{avr} [km/s]	m_p [g]	v_{avr} [km/s]	m_p [g]	v_{avr} [km/s]
62×10^6	5	5500	0.24	2.4	227	24	71.8	–	–
3.968×10^6	2	2200	0.24	0.1536	227	1.536	71.8	–	–
496×10^3	1	1060	0.23	19.2×10^{-3}	227	0.192	71.8	–	–
62×10^3	0.5	530	0.23	2.4×10^{-3}	227	24×10^{-3}	71.8	2.4×10^{-3}	227
3.968×10^3	0.2	258	0.28	153.6×10^{-6}	227	1.536×10^{-3}	71.8	153.6×10^{-6}	227
496	0.1	106	0.23	19.2×10^{-6}	227	192×10^{-6}	71.8	19.2×10^{-6}	227
62	0.05	51.2	0.23	–	–	–	–	2.4×10^{-6}	227
3.968	0.02	24.8	0.26	–	–	–	–	153.6×10^{-9}	227

III Hydrogen (H) plasma with the parameters same as the condition I: The same energies with the average velocity of 227 km/s and the mass density of 3.0×10^{-4} kg m^{-3}.

Table 1 shows the initial parameters for all conditions and all energies. We performed simulations for 8 different models for each condition. We evaluate the plasma expansion radius in a magnetic field in terms of a magnetic confinement radius $r_B = (3\mu_0 E_p/2\pi B_0^2)^{1/3}$ where B_0 is the initial ambient magnetic field [12–15] and it is proportional to $E_p^{1/3}$. The external magnetic field in our simulations at the initial plasma location is $B_c \sim 0.2$ - 0.3 T for all conditions, and therefore, the length (L) is scaled with the relation $E_p \propto L^3$, and the coil radius is in the same relation, $E_p \propto r_c^3$. Also, the plasma energy is scaled keeping the mass density in all 8 models in each condition, $E_p \propto m_p$, and therefore, v_{avr} is same for every model. Here, in the non-dimensionalized simulation without the magnetic field, the ratio of length and time scales, L/T, is generally constant, and the velocity is kept, meaning that the simulations with different energies are identical. On the other hand, with the magnetic field, the typical Larmor radius, r_{ci}, is almost the same for 8 models but it changes relative to the typical plasma scale. This means that our non-dimensionalized simulations investigate the plasma expansion depending on the ratio of r_{ci}/L, or in other words, dependence on effective field strength. In addition, we also performed simulations with two different mass density or different v_{avr} to investigate the dependence of initial conditions as shown in Table 1.

3. Result and Discussion

Figures 2(a)-2(c) show the ion density distributions at $t = 20$, 30, and 40 μs, respectively, with the energy of 62 MJ in the condition I, and Figs. 2 (d)-2(f) are those at t = 0.4, 0.6, and 0.8 μs, respectively, with the energy of 496 J in the condition I. Figures 2(g)-2(i) show the ion density distributions at $t = 1.2$, 1.8, and 2.4 μs, respectively, with the energy of 496 J in the condition II, and the plasma mass is 10 times larger than that in the condition I. The position of $(x, y, z) = (0, 0, 0)$ is the initial position of the plasma and the plasma is exhausted toward z-direction. Although the energy of 62 MJ is 50^3 times larger than that of 496 J, the spatial and temporal scales show only 50 times difference, showing mushroom-like shapes in both energies, as shown in Figs. 2 (a)-2(c) and Figs. 2 (d)-2(f). This is why the initial expansion velocity is almost same for both energy conditions with 50 times different spatial scales. In addition, the density distribution with 10 times larger density [Figs. 2 (g)-2(i)] show identical shape to those with smaller density [Figs. 2 (d)-2(f)], but in 3-times longer time-scale. These results suggest that the plasma structure is either determined only by the plasma energy and magnetic field energy, or the ratio of magnetic field energy to the plasma energy as previously discussed [5].

Figures 3(a)-3(d) show the momentum efficiency (η), specific impulse (I_{sp}), impulse bit (I_b) and normalized impulse bit ($I_b/\sqrt{m_p}$), respectively. The impulse bit, I_b, is derived by adding up the momentum of all super-particles,

$$I_b = \sum m v_{iz}. \tag{11}$$

η is the ratio of momentum in the z-direction to the initial momentum at $t = 0$ as

$$\eta = \frac{\sum m v_{iz}}{\sum |m v_{i0}|} = \frac{I_b}{\sum |m v_{i0}|}. \tag{12}$$

In addition, Eq. (10) is also expressed as

$$E_p = \sum \frac{m_i v_{i0}^2}{2} = \frac{N}{2} m_i \frac{\sum v_{i0}^2}{N} = \frac{N}{2} m_i \langle v_{i0}^2 \rangle \simeq \frac{N}{2} m_i \left[\langle |v_{i0}| \rangle^2 + \sigma_{|v_{i0}|}^2 \right], \tag{13}$$

where N is the total number of super-particles, $\langle\rangle$ indicates the expected values, and σ is the standard deviation. Using Eqs. (12) and (13), the momentum efficiency is also expressed in terms of the energy,

$$\eta = \frac{I_b}{\sqrt{2 m_p E_p - m_p^2 \sigma_{|v_{i0}|}^2}}. \tag{14}$$

The specific impulse, I_{sp}, is obtained by dividing the thrust by the mass flow rate of the propellant and expressed

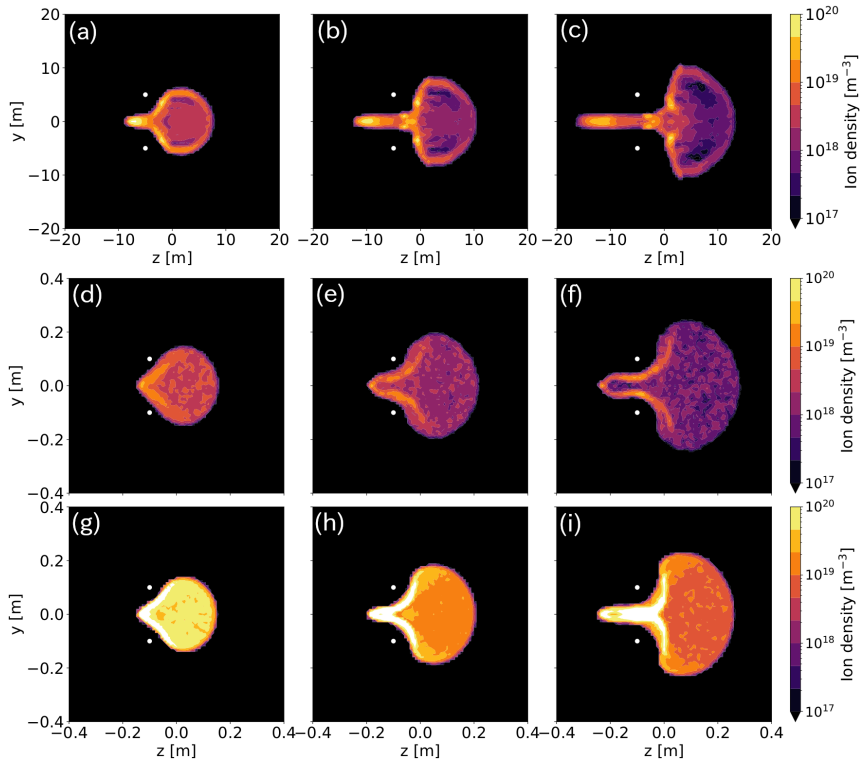

Fig. 2 The time evolution of the ion density distributions at (a) t = 20, (b) 30, and (c) 40 μs with E_p = 62 MJ in the condition I, those at (d) t = 0.4, (e) 0.6, and (f) 0.8 μs with E_p = 496 J in the condition I, and those at (g) t = 1.2, (h) 1.8, and (i) 2.4 μs with E_p = 496 J in the condition II. The white dots represent the cross-section of the magnetic coil.

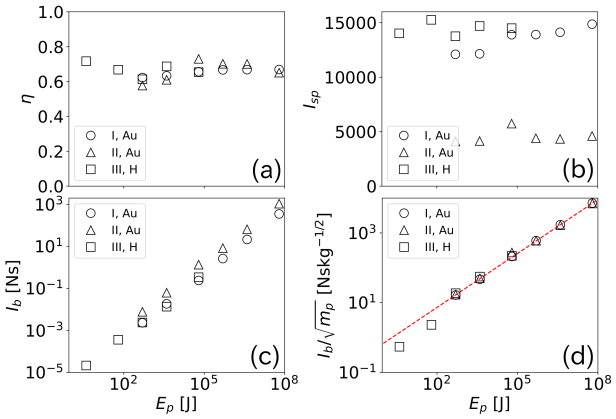

Fig. 3 (a) The momentum efficiency, η, (b) specific impulse, I_{sp}, (c) impulse bit, I_b, and (d) $I_b/\sqrt{m_p}$. The values obtained from the conditions I-III are shown with circles, triangle, and squares, respectively.

as

$$I_{sp} = \frac{\sum m v_{iz}}{m_p g}, \tag{15}$$

where g is the gravitational acceleration. These values are estimated when they are saturated, for example, at t = 80, 10, and 0.8 μs in the cases of E_p = 62 MJ, 496 kJ, and 62 J, respectively, as in a same manner in Ref. [5]. $\eta \sim 0.65$ for the cases of E_p = 496 J - 62 MJ for the Au plasma, and for E_p = 3.968 J - 62 kJ for H plasma, which is more or less same as the previous research with E_p = 4 MJ [5].

The momentum efficiency does not depend on the plasma mass and plasma energy as shown in Fig. 3 (a). The specific impulse also does not depend on the energy in all conditions (I, II, or III), but depends on the plasma mass as shown in Fig. 3 (b). Here, the specific impulse goes as $I_{sp} \sim m_p^{1/2}$. The impulse bit is expressed as a power-law of the energy and the absolute value is dependent on the plasma mass as expressed in Fig. 3 (c). Ten times larger mass generates about three times larger impulse, while the specific impulse, I_{sp}, decreases by three times. This tendency can be seen in Figs. 3 (b) and 3(c). These results also suggest that I_b is expressed with the power-law of E_p and m_p. If an exact power law can be determined, the propellant mass can be sized according to the thrust needed, allowing the propellant mass to be sized to each mission requirement. By fitting all data in Fig. 3 (d), we can obtain the following relation:

$$\frac{I_b}{\sqrt{m_p}} \sim 0.68 E_p^{0.52}. \tag{16}$$

In the case of E_p = 62 MJ and m_p = 2.4 g, v_{max} = 293 km/s and $\sigma_{|v_{i0}|}$ = 56.7 km/s, and therefore $m_p \sigma^2_{|v_{i0}|}/2E_p = 0.062$, meaning that I_b is more or less proportional to $\sqrt{m_p E_p}$ [see Eq. (14)] and the obtained index of 0.52 is consistent with

that of 0.5 estimated with small velocity deviation. This result suggests that I_b can be estimated with any material and mass using model experiments and the scaling-law of Eq. (16).

In the simulations with H plasma in the high energy region: $E_p \gtrsim 500$ kJ, the plasma is unstable in the magnetic nozzle as it expands, and the thrust performance can not be estimated reliably. In general, the hybrid simulation analyzes the spatial scale on the order of an ion inertial length as discussed in [16]. In our simulation, $\Delta x \gtrsim 0.2c/\omega_{pi}$ and the ratio of E_p/m_p is constant for all models in each condition. The ion Larmor radius (r_{ci}) becomes smaller than the grid spacing Δx as the energy and the magnetic field strength increase. Therefore, the spatial resolution may be poor in H-ion high-energy conditions due to small $r_{ci}/\Delta x$, which allows numerical instability to grow rapidly. On the other hand, the simulation with low-energy Au plasma can not be calculated correctly due to the violation of CFL condition because of small Δx and relatively large expansion velocity, or r_{ci} may be too large compared with typical plasma size. Therefore, all data in Table 1 only use stable simulation models.

4. Summary

We performed simulations to investigate the energy dependence on the thrust performance of a magnetic nozzle for a laser fusion rocket. We looked at energies ranging from $E_p = 3.968$ J to 62 MJ with the propellants of Au and H plasmas by changing the spatial scale or coil radius as $L \propto E_p^{1/3}$. Momentum efficiency of 0.6 - 0.7 were obtained at various plasma energies, and we find the momentum efficiency does not depend on the plasma energy, mass, or material. The impulse bit and normalized impulse bit are expressed as the power-law of the energy. These results suggest that the impulse bit for the laser fusion rocket can be estimated and optimized for various missions using the scaling-law obtained here.

Acknowledgments

This work was partly achieved through the use of computer resource offered under the category of General Project by Research Institute for Information Technology, Kyushu University. We would like to thank N. Schilling for helpful comments and valuable suggestions. This research was partially supported by JSPS KAKENHI grant number JP21K18176, and by the joint research project of IHI Aerospace Co. Ltd.

[1] J. Cassibry, R. Cortez, M. Stanic, A. Watts, W. Seidler, R. Adams, G. Statham and L. Fabisinski, Case and development path for fusion propulsion, J. Spacecr. Rockets **52**, 595 (2015).

[2] C.D. Orth, VISTA – a vehicle for interplanetary space transport application powered by inertial confinement fusion, Ucrl-Tr-110500 (2003).

[3] R. Hyde and J. Nuckolls, Prospects for rocket propulsion with laser-induced fusion microexplosions, In 8th Joint Propulsion Specialist Conference, Reston, Virigina (1972).

[4] R.A. Hyde, Laser-fusion rocket for interplanetary propulsion, In International Astronautical Federation conference, Budapest, Hungary (1983).

[5] Y. Nagamine and H. Nakashima, Analysis of plasma behavior in a magnetic thrust chamber of a laser fusion rocket, Fusion Sci. Technol. **35**, 62 (1999).

[6] A. Maeno, N. Yamamoto, S. Fujioka, Y. Mori, A. Sunahara, T. Johzaki and H. Nakashima, Analysis of laser wavelength and energy dependences of the impulse in a magnetic thrust chamber system for a laser fusion rocket, Trans. Jpn. Soc. Aeronaut. Space Sci. **56**, 170 (2013).

[7] T. Morita, N. Yamamoto, R. Kawashima, N. Saito, M. Edamoto, S. Fujioka, Y. Itadani, T. Johzaki, S. Miura, Y. Mori, H. Nishimura, A. Sunahara, A. Yogo and H. Nakashima, Plasma structure and energy dependence in a magnetic thrust chamber system, J. Phys. Conf. Ser. **717**, 012071 (2016).

[8] T. Ise, Concept design of laser fusion rocket, J. Plasma Fusion Res. **97**, 623 (2021).

[9] E.J. Horowitz, D.E. Shumaker and D.V. Anderson, QN3D: A three-dimensional quasi-neutral hybrid particlein-cell code with applications to the tilt mode instability in field reversed configurations, J. Comput. Phys. **84**, 279 (1989).

[10] D.S. Harned, Quasineutral hybrid simulation of macroscopic plasma phenomena, J. Comput. Phys. **47**, 452 (1982).

[11] T. Ise, Mission design of laser fusion rocket, J. Plasma Fusion Res. **97**, 621 (2021).

[12] B.H. Ripin, E.A. McLean, C.K. Manka, C. Pawley, J.A. Stamper, T.A. Peyser, A.N. Mostovych, J. Grun, A.B. Hassam and J. Huba, Large-Larmor-radius interchange instability, Phys. Rev. Lett. **59**, 2299 (1987).

[13] G. Dimonte and L.G. Wiley, Dynamics of exploding plasmas in a magnetic field, Phys. Rev. Lett. **67**, 1755 (1991).

[14] S.A. Nikitin and A.G. Ponomarenko, Dynamics and spatial boundaries of retardation of the plasma cloud of an explosion in a dipole magnetic field, J. Appl. Mech. Tech. Phys. **34**, 745 (1993).

[15] M. VanZeeland and W. Gekelman, Laser-plasma diamagnetism in the presence of an ambient magnetized plasma, Phys. Plasmas **11**, 320 (2004).

[16] D. Winske, L. Yin, N. Omidi, H. Karimabadi and K. Quest, Hybrid simulation codes: Past, present and Future –A tutorial in *Space Plasma Simulation* (Springer, 2003) pp. 136-165.